ADVANCED FUNCTIONAL MATERIALS
www.afm-journal.de

Organelle-Specific Anchored Delivery System Stretching a Reversal of Tumor Hypoxia Microenvironment to a Combinational Chemo-Photothermal Therapy

*Xuerui Chen, Xuelian Yin, Lin Zhan, Junfeng Zhang, Yuxi Zhang, Yinghua Wu, Jiale Ju, Yajie Li, Qianghua Xue, Xu Wang, Chenchen Li, Rui L. Reis, and Yanli Wang**

Direct delivery to an organelle-specific point can boost the efficacy of therapy procedures to new heights. Among other subcellular organelles, mitochondria generate ATP as intracellular powerhouse, and are associated with multiple aspects of tumorigenesis and tumor development. Here, a mitochondrial anchored biomimetic nanoplatform (CZACN) is designed and its reversal of tumor hypoxia microenvironment underlying the mitochondria-located chemo-photothermal therapy is studied. After shuttling into cancer cells, therapeutic payloads including cisplatin (CDDP) and Au nanozymes are controllably released in the ATP-overexpressed mitochondria. CDDP generates $O_2^{\bullet -}$, forms H_2O_2 for a chemical fuel in the next reaction, and damages mitochondrial DNA. Meanwhile, the catalase-like Au nanozymes catalyze the produced hydrogen peroxide for oxygen supply to relieve hypoxic tumor microenvironment, offering cytotoxic singlet oxygen against cancer cells under NIR treatment. As a result of cancer-cell self-recognition, mitochondria-targeted therapy, and photothermal conversion ability, the fabricated CZACNs obtained 89.2 ± 3.70% of tumor growth inhibition under NIR irradiation and constrained the dose-limiting toxicity of CDDP, as well. These findings reinforce the synergistic effect of organelle-specific navigation and in situ oxygen self-sufficiency for combinational chemo-photothermal therapy.

1. Introduction

Recent developments in conventional targeted delivery systems are mainly focused on cell-membrane targeting throughout the delivery to pathological tissues and release in the cytoplasm.[1] Delivery systems can first arrive at tumor tissues via the enhanced permeation and retention (EPR) effect.[2] They traverse a series of biological barriers to accumulate at a particular organelle (nucleus, Golgi apparatus, mitochondria, endo/lysosome, etc.) to work. However, only a small fraction of therapeutic payloads successfully reaches the organelle-specific point. For example, it was reported that behind 0.1% of DNA in the cytoplasm can be expressed in the nucleus.[3] Therefore, direct delivery to subcellular organelles is a key step to tackle the high dosage requirements and systemic toxicities caused by the lack of specificity.[4]

Compared with other organelles in eukaryotic cells, mitochondria with bilayer membrane serve as a powerhouse and weapon store to generate ATP for cells. Beyond energy production, they participate in a variety of biological activities, ranging from reactive oxygen species (ROS), mitophagy, metabolism, homeostasis, and apoptosis.[5]Moreover, mitochondria are verified to be susceptible to hyperthermia, which present an opportunity for photothermal therapy.[6] Mitochondria-specific delivery is an applicable strategy to increase the treatment efficiency. Several methods have been implemented for mitochondrial anchored delivery systems, including nanoplatforms modified by delocalized lipophilic cations, positively charged amphiphilic molecules, or

X. Chen, X. Yin, L. Zhan, J. Zhang, Y. Zhang, Y. Wu, J. Ju, Y. Li, Q. Xue, C. Li, R. L. Reis, Y. Wang
Tumor Precision Targeting Research Center
School of Medicine & School of Environmental and Chemical Engineering
Shanghai University
Shanghai 200444, China
E-mail: wangyanli@staff.shu.edu.cn

X. Yin, L. Zhan, J. Zhang, Y. Zhang, Y. Wu, J. Ju, Y. Li, Q. Xue, C. Li, Y. Wang
Institution of Nanochemistry and Nanobiology
School of Environmental and Chemical Engineering
Shanghai University
Shanghai 200444, China

The ORCID identification number(s) for the author(s) of this article can be found under https://doi.org/10.1002/adfm.202108603.

X. Wang
Hangzhou Medical College
Binjiang Higher Education Park, Binwen Road 481, Hangzhou 310053, China

R. L. Reis
3B's Research Group—Biomaterials, Biodegradables and Biomimetics
University of Minho
Headquarters of the European Institute of Excellence on Tissue Engineering and Regenerative Medicine
Ave Park, 4805-717 Barco, Guimarães, Portugal

R. L. Reis
ICVS/3B's—PT Government Associate Laboratory
Braga/Guimarães, Portugal

DOI: 10.1002/adfm.202108603

mitochondrial targeting signal peptide, respectively.[1,7]Among them, mitochondrial-targeted nanomedicines such as Szeto–Schiller peptides have been initiated, but has yet to result in clinical validation and approval because of their uncertain metabolism in tissues.[8]

According to the above obstacles, we designed a mitochondrial-targeted nanoplatform (CZACN). It is composed of ZIF-90 for mitochondria-specific delivery, cancer cell membrane coating for immune system and homologous target, cisplatin (CDDP) for chemotherapeutics, and Au nanozymes for oxygen self-sufficiency as well as photothermal therapy. The ZIF-90 emerges from other metal organic frameworks with a characteristic sensitivity to the high ATP-dose environment, due to its structural disintegration caused by competitive coordination of ATP and zinc.[9] It benefits controllable release of the payloads in mitochondria where the ATP dose is almost 25-folds higher than that in the extracellular environment.[10] The zinc ions dissociated from ZIF-90 would stimulate ROS generation, eventually leading to apoptosis.[11]Further coated by cancer cell membranes, the ZIF-90 is provided with the protein and antigenic diversities replicated from cancer cell membranes on its surfaces, thus it can escape from the immune system and target homologous tumors.[12]CDDP is one of the typical platinum-based drugs, whose interaction with nucleus DNA forms Pt-DNA adducts to cut off the gene replication and transcription, eventually causing apoptosis and cell death. It can activate NADPH oxidases, generate $O_2^{\bullet -}$, and produce H_2O_2 in cancer cells.[13] Whereas, CDDP is currently compromised by tumor hypoxic microenvironment which negatively affects the formation of Pt-DNA adducts, thus complicated by its dose-limiting toxicities.[14] To relieve tumor hypoxic microenvironment, we select Au nanozymes to be coloaded by ZIF-90, which have enzyme mimetic catalytic characteristics and exceed natural catalase in catalysis and stability.[15] They can catalyze excessive H_2O_2 to produce O_2 and singlet oxygen ($^1O_2$) under NIR irradiation to alleviate tumor hypoxia and promote strong toxicity toward cancer cells. In addition, Au nanozymes feature excellent photothermal conversion efficacy under irradiation of laser (650–1100 nm).[16]

Therefore, we envisage that the biomimetic ZIF-90 delivery system can be harnessed to ameliorate the inherent limitations of CDDP and create an in situ $^1O_2$ production in mitochondria to surmount its short lifetimes (<40 ns) and a small action range (<20 nm).[17] CZACNs were afforded with O_2 self-sufficiency, organelle-specific release, and photothermal conversion properties. Besides, mild hyperthermia at 52 °C under NIR irradiation can enhance their permeability and fluidity, eventually increasing their intracellular accumulation.[18] As a result, the proof-of-concept findings facilitate the corporation of mitochondria-specific delivery and tumor hypoxia modulation in enhancing efficiency of chemo-photothermal therapy.

2. Results and Discussion

2.1. Synthesis and Characterization of CZACNs

The preparation of CZACN composite using a biomimetic mineralization approach is illustrated in **Figure 1**a. Thanks to the well-organized structure of ZIF-90 with the size of pore (11.2 Å) and window (3.5 Å), CDDP with nonplanar structure in 3D can be exactly encapsulated inside of ZIF-90, thus forming CDDP@ZIF-90 nanoparticles (NPs). Next, catalase-like Au nanozymes are embedded in the nanoscaled ZIF-90 for the synthesis of CZAu NPs. Finally, mouse breast cancer cell (4T1 cells) membrane fragments coat CZAu NPs by extrusion to obtain CZACNs. The TEM image of CZACNs exhibits a representative core-shell structure of 125 ± 32 nm as expected with a cancer cell membrane coating (Figure 1b). Different contrast from the ZIF-90 shell in Figure 1c and Figure S2d, Supporting Information, identifies that the CZAu NPs are embellished by Au nanozymes. FTIR spectra analyzed structures of the fabricated nanoplatforms. CZAu NPs and CDDP@ZIF-90 NPs exhibit strong absorption peaks at 1640 and 1100 cm^{-1} belonging to the $^-NH_2$ vibration of CDDP. A characteristic peak at 2820 cm^{-1} attributed to the −C=O of ZIF-90 also appears both in the spectra of CDDP@ZIF-90 and CZAu NPs (Figure 1d). In addition, the UV–Vis spectra of CDDP@ZIF-90 and CZAu NPs are consistent with that of free CDDP (Figure 1e). Results from FTIR and UV–Vis imply that CDDP is effectively encapsulated inside of ZIF-90. Zeta potential characterizations demonstrate that CZACNs possessed a negative surface charge from Au nanozymes and cancer cell membrane, which is beneficial to the immune escape and avoided aggregation in blood (Figure 1f). Sizes of CZACNs detected by DLS are larger than those of CZAu NPs (110 ± 23 nm) and CDDP@ZIF-90 NPs (83 ± 28 nm), partly resulted from the embedding of Au nanozymes and coating of cell membrane (Figure 1g). The content of Au in CZACN detected by EDS was 9.85%. X-ray diffraction (XRD) data further reveals their same crystalline forms as ZIF-90 alone, demonstrating that further modification by CDDP encapsulation, Au nanozymes embellishment and cancer cell membrane coating did not change the diffraction peaks of standard ZIF-90 (Figure 1h). Thermal stabilities of CZACN, CZAu, ZIF-90, and CDDP@ZIF-90 NPs were characterized by TGA in nitrogen (Figure S4, Supporting Information). It reveals that the incorporation of CDDP and Au nanozymes into the ZIF-90 does not change the thermal stability. As illustrated in Figure 1n, the protein profiles of CZACNs and 4T1 cell membranes seem the same, indicating that adhesion protein molecules of 4T1 cell membrane are transferred to CZACNs and benefit the special bindings to cancer cells. The EDS elemental mappings of the elements (O, Zn, and Au) from the CZACNs and CZAu NPs suggest an effective synthetic process for CZACNs and CZAu NPs (Figure 1o and Figure S1, Supporting Information). With the UV–Vis absorbance in 302 nm (Figure S5, Supporting Information), the CDDP loading efficiency in NPs was calculated as 24.94%. To analyze their solubility in water, CZACNs were immersed in D.I. water for 72 h and 100 µL of solution was taken out for UV–vis detection every 24 h. We found the peak at 286 nm attributed to ZIF-90 always present in CZACN solution till 72 h while the peaks of CDDP and Au nanozymes were invisible in CZACN solution (Figure S6, Supporting Information). Results above imply that none of the component was separated from CZACN due to its low solubility in D.I. water. To figure out the biosafety of CZACN, we specially studied its stability in blood, serum, and saline by UV–Vis. After monitoring

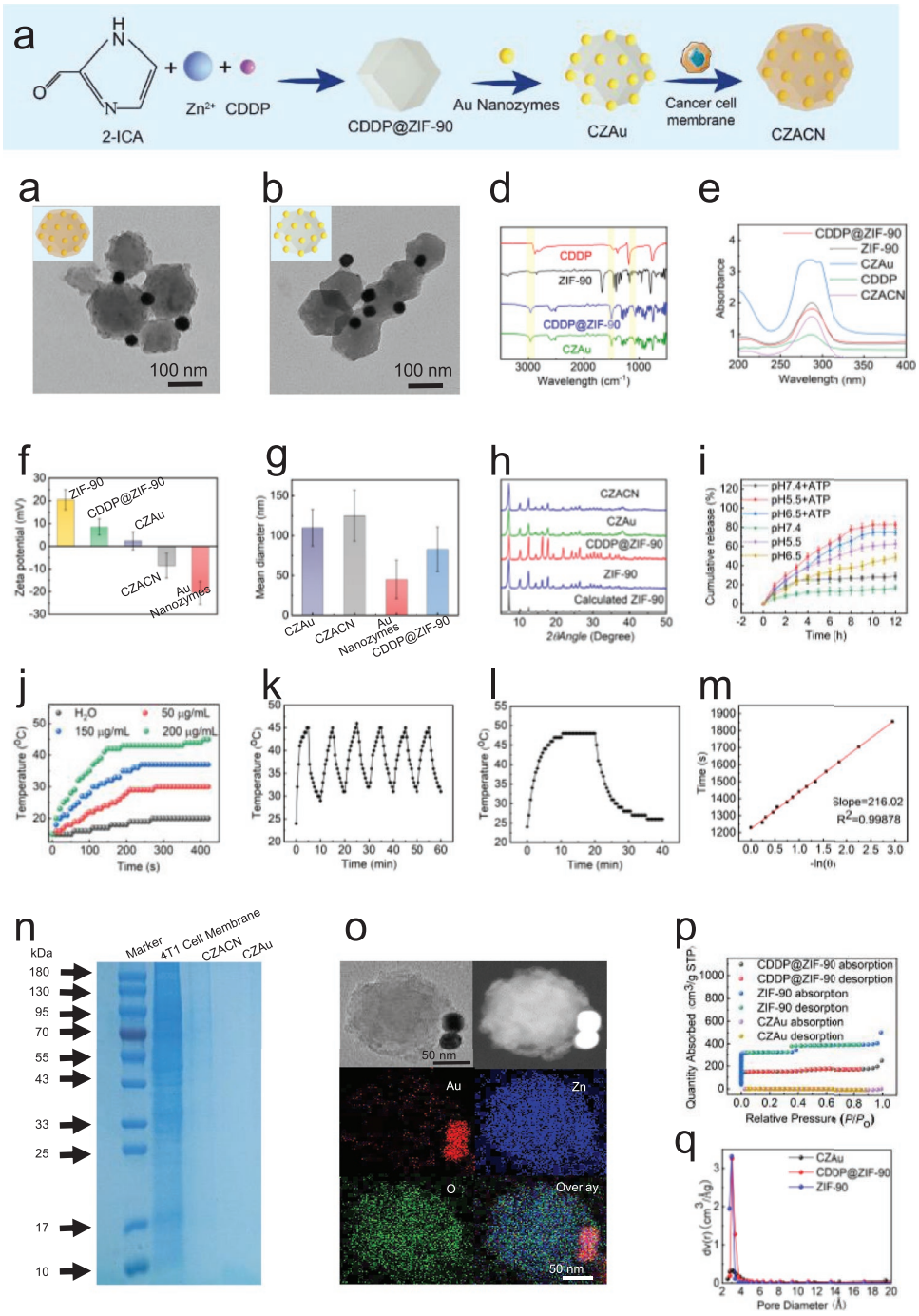

Figure 1. Characterization of mitochondrial anchored CZACNs. a) Illustration of CZACNs preparation; b) TEM image of CZACNs; c) TEM image of CZAu NPs; d) FTIR spectra of CDDP, ZIF-90, CDDP@ZIF-90, and CZAu NPs; e) UV–Vis spectra of CDDP, ZIF-90, CDDP@ZIF-90, CZAu NPs, and CZACNs; f) zeta potential of ZIF-90, CDDP@ZIF-90, CZAu NPs, CZACN, and Au nanozymes; g) Hydrodynamic size distribution of CZAu, CZACN, CDDP@ZIF-90 NPs, and Au nanozymes; h) XRD patterns of ZIF-90, CDDP@ZIF-90, CZAu, and CZACNs; i) pH and ATP triggered drug release of CZACNs in PBS of pH 5.5, 6.5, and pH 7.4; j) Temperature curves of H_2O and H_2O containing CZACNs (50–200 μg/mL) after being exposed to laser of 808 nm (2.0 W cm^{-2}); k) Photothermal stability of CZACN (10 mg/mL) in six consecutive photothermal heating (2.0 W cm^{-2}) and natural cooling cycles; l) Temperature profile of CZACN (10 mg/mL) under photothermal heating and natural cooling process in a quartz cuvette in 40 min; m) Plot of time versus negative natural logarithm of the temperature driving force ($\frac{\Delta T}{\Delta T_{max}}$) in the natural cooling process; n) SDS-PAGE protein analysis of 4T1 cell membrane, CZACN, and CZAu NPs; o) Elemental mapping of CZACN; p) N_2 adsorption–desorption isotherms of ZIF-90, CDDP@ZIF-90, and CZAu NPs; q) Pore diameter of ZIF-90, CDDP@ZIF-90, and CZAu NPs.

the UV–Vis absorbance in blood, serum, and saline for 72 h, we found the characteristic peak of ZIF-90 at 286 nm unchanged in all three solutions which demonstrates superior stability of CZACN in blood, serum, and saline (Figure S7, Supporting Information). The surface areas of CDDP@ZIF-90 and CZAu NPs were found decreased because of the CDDP encapsulation and Au nanozymes embellishment on ZIF-90 (Figure 1p,q).

Then, we exploited the ATP-sensitive property of CZACNs in response to ATP and NIR irradiation (Figure 1i). Release of CDDP from CZACNs was monitored in conditions of pH 7.4, 6.5, and pH 5.5 at 37 °C for 12 h, in which pH 7.4, 6.5, and 5.5 mimic normal tissues, tumor microenvironment and tumor tissues, respectively. In the PBS of pH 7.4 containing 0.5 mM of ATP, release percent of CDDP was 29.2 ± 3.7% after 12 h, which exceeded 11.9 ± 1.7% than that in PBS of pH 7.4. Approximately 63.3 ± 4.3% and 82.9 ± 3.1% of CDDP were released from CZACNs in PBS of pH 5.5 and PBS of pH 5.5 containing 0.5 mM ATP at 12 h, respectively. When located in tumor microenvironment of pH 6.5, CZACNs were observed to release 48.8 ± 3.9% of CDDP during 12 h. Degradation of CZAu NPs in an acidic environment (pH 6.5) containing 0.5 mM of ATP was evidenced by TEM imaging (Figure S3, Supporting Information), which displayed partial swelling and melting of CZAu NPs. It suggested that the CZAu NPs and CZACNs could maintain stability in neutral conditions, but quickly degrade in an acid microenvironment, particularly in the mitochondria with relatively high ATP levels. As illustrated in Figure 1j, CZACNs showed a concentration-dependent photothermal response under NIR irradiation, in comparison with a negligible temperature increase of water. The CZACN presented similar behavior in six consecutive heating and cooling cycles, demonstrating CZACN has a photothermal stability and 24.1% of photothermal conversion efficiency according to Equations (1) and (2) in Figure 1k–m. Results above demonstrate that CZACNs were designed with ATP-sensitivity and photothermal conversion ability.

2.2. Chemo-Photothermal Therapy of CZACNs Against Tumor In Vivo

We performed all animal experiments following "The National Regulation of China for the Care and Use of Laboratory Animals" and were approved by the Institutional Animal Care and Use Committee of Shanghai University.

As we expect, the mechanism of chemo-photothermal therapy in CZACNs involves following parts (**Figure 2**a). Inner CDDP is released in the mitochondria and activates Pt-DNA adducts to generate H_2O_2. Au nanozymes catalyze H_2O_2 to produce O_2 for modulation of tumor hypoxia microenvironment, in which the coproduct $^1O_2$ generates toxicity to cancer cells. Meanwhile, Au nanozymes transfer the irradiation to hyperthermia for photothermal therapy. Thus, we emphatically investigated how the catalase-like Au nanozymes and NIR irradiation synergistically fueled CZACNs against the heterogenous tumor of 4T1. Results of tumor weight validated the outstanding therapeutic outcome of CZACNs (administration dosage 6 mg/kg) under NIR irradiation (2.0 and 1.0 W cm^{-2}), whose group had the lightest tumor weight (Figure 2d,k). The tumor growth inhibition (TGI) rate of the CZACN+laser group (laser power 2.0 W cm^{-2}, 2 min) was limited to 89.2 ± 3.7%, the highest TGI of all treatments (Figure 2g). Under NIR irradiation (2.0 W cm^{-2}, 2 min), CZAu NPs also showed moderate anticancer capability (TGI 79.0 ± 4.80%). In addition, The TGIs of CZACN+laser group and CZAu+laser group under irradiation of laser (808 nm, 1.0 W cm^{-2}, 2 min) were 69.4 ± 6.9% and 51.7 ± 29.7%, respectively. The gap between CZAu group and CZACN group is mainly due to effective cancer cell membrane coating on the surface of CZACNs, suggesting that cancer cell membrane coating endows the NPs with homologous target and immune escape. Significant negative effects ($p < 0.01$) were displayed in the body weights of mice treated with CDDP (administration dosage 1.5 mg/kg), compared with that in the saline group during the therapeutic period, indicating high toxicity of CDDP (Figure 2f). It was also found that the Zn contents from CZACN in urine increased gradually after 4 h of injection while the Zn contents of urine maintained unchanged after injection of normal saline (Figure 2e). Their significant differences were attributed to the metabolism of CZACN in mice.

After administration of normal saline, CZACNs, and CZAu NPs for 24 h, tumor-bearing mice were also taken photos by thermal infrared imaging camera for photothermal imaging. The temperature of saline-treated mice increased slightly after laser irradiation (808 nm, 2.0 W cm^{-2}) for 2 min (**Figure 3**b). CZACNs-treated mice showed a rapidly increased local temperature to 52.2 °C within 2 min under NIR irradiation, according to the targeted accumulation and photothermal conversion property of CZACNs at tumor site. Apoptosis levels of tumors analyzed by TUNEL, GPX4, and Ki67 expressions by immunohistochemical (IHC) further reveal the mechanism of synergistic therapy (Figure 3a). We found obvious apoptosis in tumors of CZACNs+laser, which was further revealed by decreased GPX4 expression and Ki67-positive cells. These results implied that CZACN could effectively inhibit tumor growth by inducing apoptosis and ferroptosis under NIR irradiation. It might be resulted from the activation of NADPH oxidases and the formation of $NADP^+$ by CDDP which is controllably released in mitochondria to generate Pt-DNA adducts. Then, the hypoxia status of tumors was assessed using an IHC staining assay of HIF-1α. The HIF-1α staining of tumors in CDDP and CDDP@ZIF-90 group showed little difference compared to that of the saline group, indicating the tumor hypoxia without improvement. In contrast, HIF-1α positive signals were shown in tumor slices after CZAu or CZACN treatment, demonstrating the relieved tumor hypoxia. It is mainly ascribed to the catalase-like activity of Au nanozymes, which could decompose the up-regulated H_2O_2 in the tumor region to relieve inner hypoxia of the tumor. We concluded that the CDDP and Au nanozymes released from CZACNs synergistically induced apoptosis to inhibit tumor growth and relieve tumor hypoxic microenvironment.

2.3. Mitochondria-Targeted Mechanism of CZACN In Vitro

To deeply investigate the enhanced therapy efficiency of CZACNs, we narrowed down the organelle-specific target to mitochondria. As illustrated in Figure S8, Supporting Information, ZIF-90 NPs negligibly affected cell proliferation in the detected concentrations, implying ZIF-90 NPs with a satisfied biocompatibility. The cytotoxicities of CDDP and CDDP@ZIF-90 were analyzed by treating 4T1 cells, HepG2 cells, and

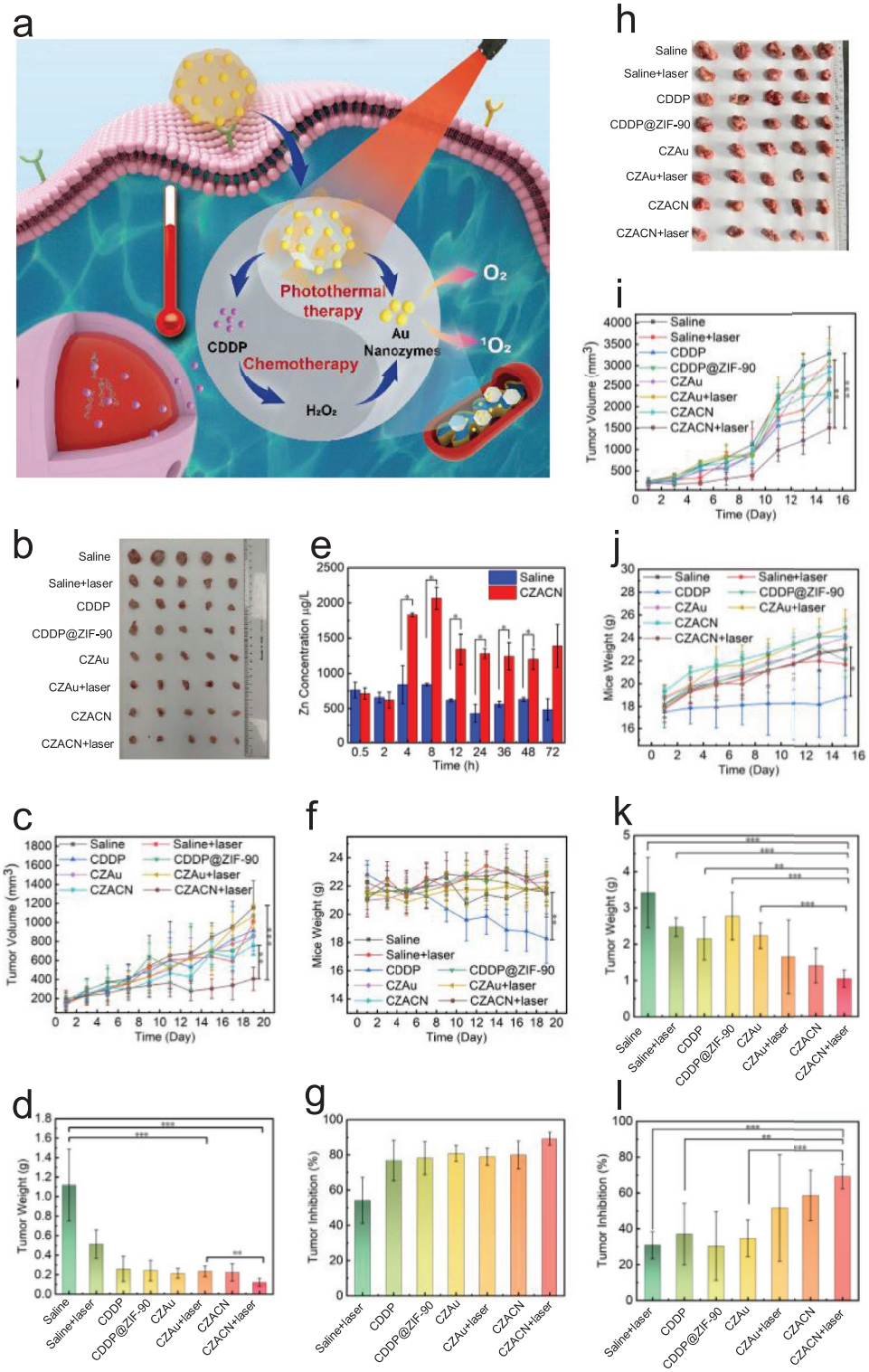

Figure 2. Antitumor therapy of CZACN for Balb/c mice in vivo (dosage of CDDP 1.5 mg/kg). a) Schematic illustration of CZACNs for combinational chemo-photothermal therapy; b) Photographs of the tumor dissection (laser irradiation: 2.0 W cm^{-2}, 2 min); c) Tumor volumes of mice after being treated with various groups (laser irradiation 2.0 W cm^{-2}, 2 min); d) Tumor weight of mice in various groups (laser irradiation 2.0 W cm^{-2}, 2 min); e) Zn concentration of urine from mice after injection of CZACN or saline; f) Mice weight of various groups (laser irradiation 2.0 W cm^{-2}, 2 min); g) Tumor inhibition of mice in various groups (laser irradiation 2.0 W cm^{-2}, 2 min); h) Photographs of the tumor dissection (laser irradiation: 1.0 W cm^{-2}, 2 min); i) Tumor volumes of mice after being treated with various groups (laser irradiation: 1.0 W cm^{-2}, 2 min); j) Mice weight of various groups (laser irradiation: 1.0 W cm^{-2}, 2 min); k) Tumor weight of mice in various groups (laser irradiation: 1.0 W cm^{-2}, 2 min); l) Tumor inhibition of mice in various groups (laser irradiation: 1.0 W cm^{-2}, 2 min). *** indicates $p < 0.001$, ** indicates $p < 0.01$, * indicates $p < 0.05$.

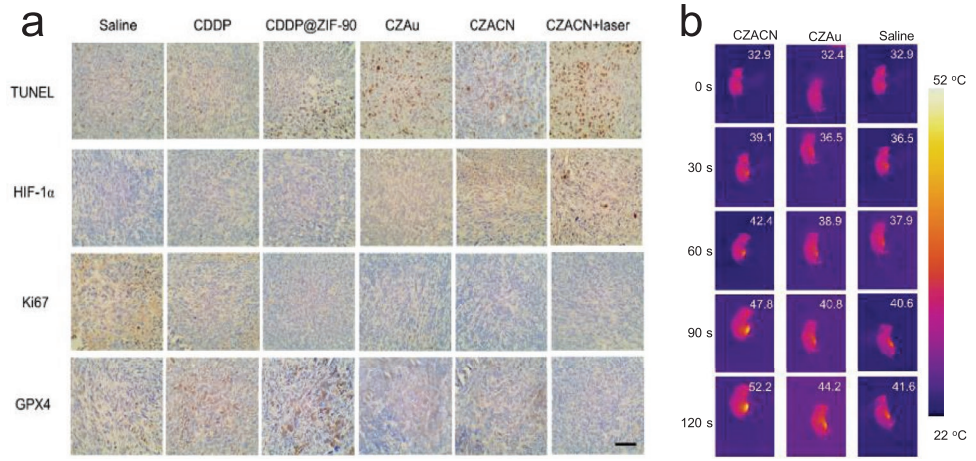

Figure 3. a) TUNEL staining, IHC staining of HIF-1α, Ki67, and CPX4 of tumors from various groups (dosage of CDDP 3 mg/kg, laser irradiation: 2.0 W cm^{-2}, 2 min), scale bar, 50 μm; b) Representative IR thermal images of tumor-bearing mice in vivo before and after the treatment with various groups (dosage of CDDP 1.5 mg/kg, laser irradiation: 2.0 W cm^{-2}, 2 min).

SW1990 cells with CDDP and CDDP@ZIF-90 NPs. The cell viability of CDDP@ZIF-90 is much lower than that of CDDP whether for 4T1 cells, HepG2 cells, or SW1990 cells. It reveals that ZIF-90 delivery is beneficial to elevate the chemotherapeutic efficiency of CDDP (Figure S9a,b, Supporting Information).

Targeting anticancer efficiency of CZACNs in vitro was assessed by comparing the viabilities of 4T1 cells, HepG2 cells, and SW1990 cells. These cells were incubated with CZACNs in parallel for 24 h. As shown in **Figure 4**a and Figure S9, Supporting Information, CZACNs prefer to inhibit viabilities of 4T1 cells compared to HepG2 cells and SW1990 cells, which are attributed to the homologous binding of 4T1 cell membrane coating to 4T1 cells. The antiproliferative effects of CZACNs for 48 and 72 h were similar to those for 24 h. The cytotoxicities of CZACNs and CZAu NPs were enhanced under 808 nm laser radiation, which states that the photothermal therapy of Au nanozymes synergistically inhibits the growth of cancer cells (Figure 4a).

Moreover, multicellular tumor spheroids (MCTS) were fabricated to simulate the status of solid tumors in vivo and investigate the penetration ability of CZACNs into the tumor (Figure 4c). The penetration ability in vitro of CZACNs was monitored by collecting fluorescence images at different depths using confocal laser scanning microscopy (CLSM). Under irradiation of 808 nm laser, the internal and edge of MCTS were labeled with green fluorescence by FITC-labeled CZACNs. In contrast, FITC-labeled CZACNs were found mainly in the periphery of the MCTS without NIR exposure. It indicates that laser irradiation accelerates the penetration of nanoplatforms into the inner area of MCTS. It could be resulted from the temperature increase under NIR exposure, which has been proved by the tracked temperature (Figure 4d). These images indicate potential penetration ability of the developed CZACNs into the internal area of solid tumors for drug delivery.

FITC-labeled CZACNs with fluorescence can be tracked to reveal the organelle-specific location of CZACNs. The FTIC-positive cells were observed under CLSM and analyzed by flow cytometry. We found the cellular uptake of CZACNs was the highest at 8 h of incubation and then decreased with incubation time increasing (Figure 4b), which was affected by the cell viability of 24 h and the intracellular metabolism of CZACNs. The pathway by which CZACNs were internalized was subsequently explored under CLSM. 4T1 cells were costained by Hochest 33 342 (cell nucleus indicator) and MitoBright LT Deep Red (mitochondria indicator) when pretreated with FITC-labeled CZACNs (Figure 4e). Mitochondria were overlaid by red fluorescence since the cells were incubated with CZACNs for 8 h, which demonstrates mitochondria-location of CZACNs. Prolonging incubation time to 24 h, we found shrinking cells, which reveals the cells were dying. Results from CLSM demonstrate the dissociation of ZIF-90 matrix in the high ATP-dose condition is suitable for mitochondrial-targeted accumulation.

After being released in mitochondria, CDDP could further interrupt expression of mitochondria DNA and form Pt-DNA adducts to affect mitochondrial membrane potential ($\Delta\Psi m$).[19] When a mitochondrial membrane depolarization occurs, JC-1 probes exist as monomers in the cytosol and emits green fluorescence. In contrast, JC-1 aggregation emits red fluorescence in the mitochondria. The CZACN-treated group exhibited a significant number of monomers (49.5 ± 4.98%) under NIR irradiation since the monomeric form of JC-1 was present in the cytosol (**Figure 5**a). Fluorescence observation by CLSM and quantitative analysis by flow cytometry confirmed that the mitochondria-target release of CDDP and Au nanozymes promoted monomer production, reflecting mitochondrial depolarization. Moreover, injured mitochondria DNA lacks a self-repair ability, resulting in an early apoptosis of cells. We employed Annexin V-FITC and PI to evaluate the effects of CZACN on apoptosis based on the crucial regulatory role of mitochondria in the intrinsic pathway of apoptosis. The proportion of apoptosis cells was 54.64%, 41.49%, 17.02%, and 6.48% after treatment with CZACN+laser, CZAu+laser, CZAu, CDDP, respectively (Figure 5b). Due to the synergistic enhancement of $^1O_2$ by Au nanozymes for apoptosis, the CZACN+laser group showed the increased potential of apoptosis under NIR radiation. Compared with the data in Figure S10, Supporting Information, the apoptosis efficiency of CZACN on 4T1 cells was relatively higher than those on HepG2 cells and SW1990

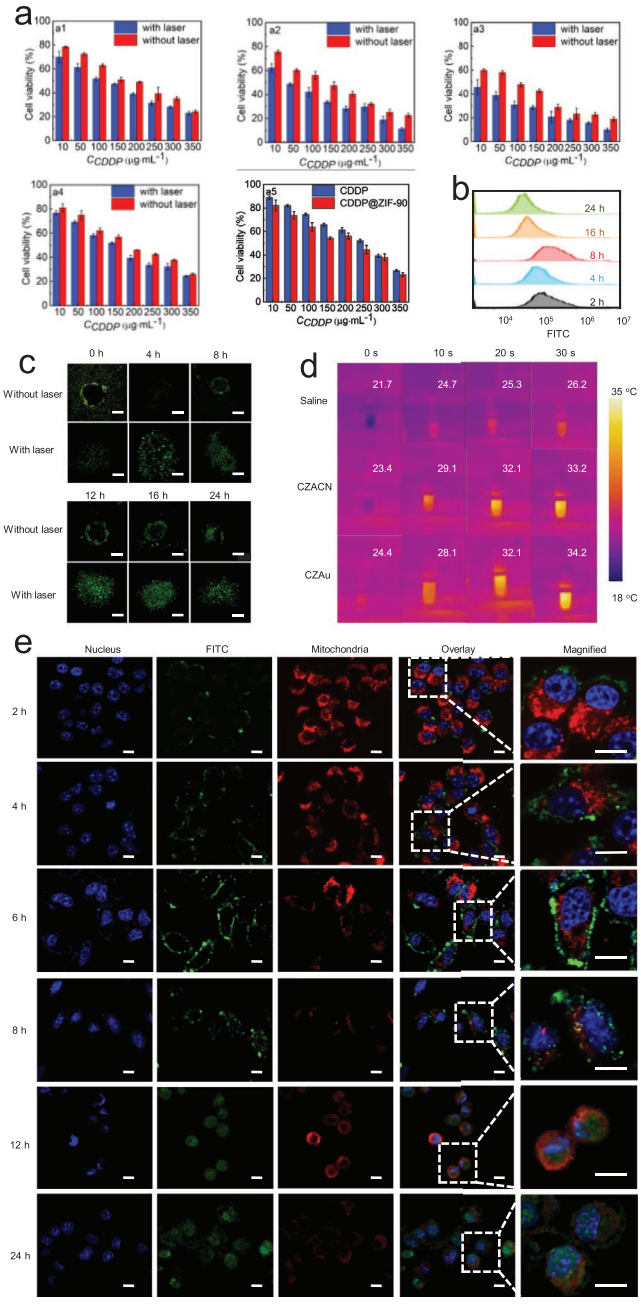

Figure 4. Targeting anticancer efficiency of CZACNs in vitro. a) 4T1 cell viability after incubation with different drugs, a1) CZACNs for 24 h, a2) CZACNs for 48 h, a3) CZACNs for 72 h, a4) CZAu for 24 h, a5) CDDP and CDDP@ZIF-90 for 24 h; b) cellular uptake of 4T1 cells treated with FITC labeled CZACNs containing equivalent CDDP concentration of 20 μg/mL analyzed by flow cytometry; c) Z-stack CLSM images of MCTS treated with FITC labeled CZACNs with or without NIR irradiation containing equivalent CDDP concentration of 20 μg/mL for 0, 4, 8, 12, 16, and 24 h, scale bar, 200 μm; d) Representative IR thermal images of different formulation dispersions with NIR irradiation for 30 s; e) CLSM images of 4T1 cells treated with FITC labeled CZACNs containing an equivalent CDDP concentration of 20 μg/mL for 2, 4, 6, 8, 12, 24 h, scale bar, 10 μm.

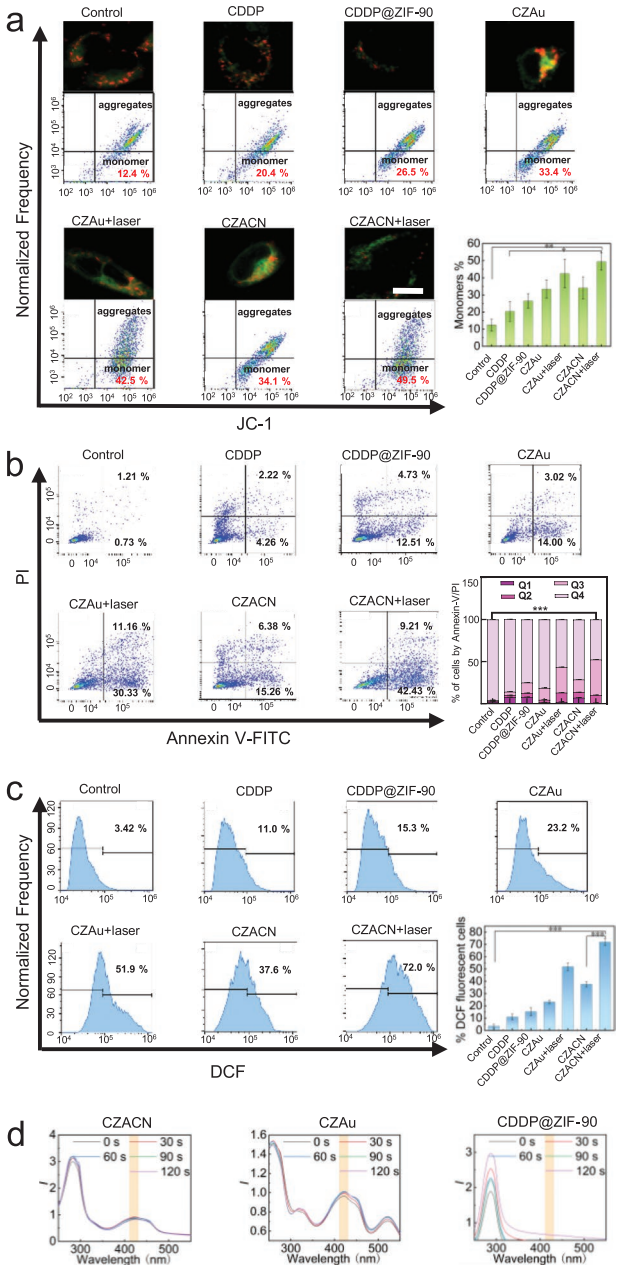

Figure 5. Death mechanism of 4T1 cells induced by the CZACNs. a) JC-1 stained mitochondrial membrane potential of 4T1 cells for 24 h treatment detected by CLSM and flow cytometry, scale bar, 10 μm; b) Apoptosis of 4T1 cells for 24 h treatment analyzed by flow cytometry; c) ROS levels of 4T1 cells for 24 h treatment analyzed by flow cytometry; d) Singlet-oxygen capture and release of CZACNs, CZAu, and CDDP@ZIF-90 with NIR irradiation for 2 min. *** indicates $p < 0.001$, ** indicates $p < 0.01$, * indicates $p < 0.05$.

cells, exhibiting a targeted cellular uptake of CZACNs which benefits from their typical proteins replicated from 4T1 cell membranes. Therefore, mitochondria target and homologous binding to cancer cells might achieve an improved therapeutic efficacy.

The higher metabolic activity and mitochondrial malfunction in cancer cells, the more hydrogen peroxide produced in cancer cells. DCFH-DA was applied in monitoring cellular ROS levels, whose product hydrolyzed by esterase can be

oxidized to DCF and emit a green fluorescence. ROS accumulation in cells incubated with CZACNs for 24 h was confirmed by strong green fluorescence after NIR irradiation. In contrast, the control group showed negligible fluorescence (Figure 5c). Furthermore, 48 h treatment of CZACNs with NIR radiation also induces excessive ROS in 4T1 cells (Figure S11, Supporting Information).

The mechanism of H_2O_2-induced ROS production is mainly from $^1O_2$ which can be detected by DPBF, an extracellular ROS indicator. Reaction with $^1O_2$ would consistently reduce the absorption intensity of DPBF at 410 nm. We investigated the singlet-oxygen generation process under CZACN, CZAu, or CDDP@ZIF-90 treatment by detection of UV–Vis every 30 s under NIR irradiation. The absorbance intensity at 410 nm of the CZACN group after irradiation of 808 nm continued to decrease during 2 min in the dark, which suggests the $^1O_2$ generation of CZACN. The reduced absorbance intensity of CZAu NPs at 410 nm also indicated CZAu NPs effectively induced intracellular $^1O_2$ generation. In contrast, negligible absorbance at 410 nm in the CDDP@ZIF-90 group was observed (Figure 5d). These are attributed to the $^1O_2$ released by Au nanozymes from CZACNs and CZAu NPs under NIR irradiation.

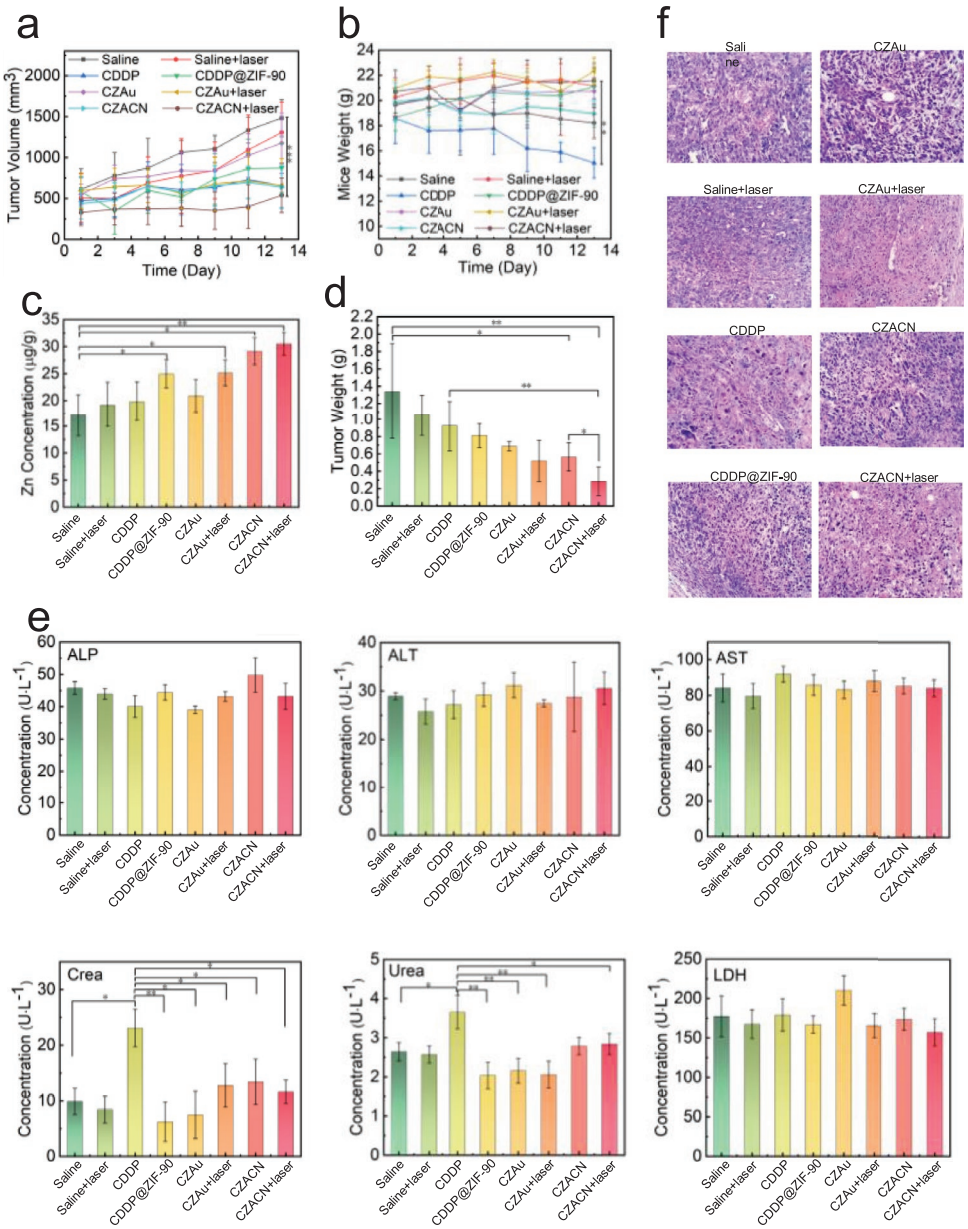

Figure 6. Reduced dose-limiting toxicity of CZACNs (dosage of CDDP 3 mg/kg) for Balb/c mice. a) Tumor volumes of mice after treated with various groups; b) Mice weight of various groups; c) Zn concentration of tumors from mice after a seven times injection. (Mean ± SD., $n = 3$); d) Tumor weight of the mice; e) Activities of typical biochemical markers of the liver and renal function. Mean ± SD., $n = 3$; f) H&E-stained tumor slices 24 h after treatments with different groups, scale bar, 50 μm. *** indicates $p < 0.001$, ** indicates $p < 0.01$, * indicates $p < 0.05$.

2.4. Reduced Dose-Limiting Toxicity of CZACNs

Almost all chemotherapeutic drugs, including CDDP, show a range of unwanted side effects due to the lack of selectivity for tumor tissue over normal tissue. The dose-limiting side effect of CDDP is nephrotoxicity, which may lead to a prescribed dose reduction in their platinum drugs of between 25 and 100%.[20] Loaded by organelle-specific nanoplatform, CDDP is directly delivered to mitochondria with its biosafety and target increased. We emphasized the dose-limiting toxicity of CZACNs with two administration dosage (6 and 12 mg/kg) in vivo. As observed in **Figure 6**a, the tumors from mice treated with saline grew rapidly, whereas the growth of those from mice treated with free CDDP (administration dosage 3 mg/kg) could be moderately inhibited. We found that CZACNs (administration dosage 12 mg/kg) were the most effective at inhibiting tumor growth when compared to other groups containing equivalent dose of CDDP (administration dosage 3 mg/kg). The tumor weight of mice reached 0.2855 ± 0.1635 g on the 13th day after 7 injections of the CZACN (administration dosage 12 mg/kg) with NIR radiation (Figure 6d).

The biodistributions of CZACN in major normal organs were analyzed by ICP-OES, while the lesions or abnormalities in normal organs were observed by H&E staining. After administration, the NPs were redistributed to organs by blood circulation, some of which were cleared and others left in the organs. We aim to analyze the zinc distributions in different organs to figure out their biodistributions in normal organs and tumors, respectively. Accumulated zinc doses in these normal organs show little difference among all groups (whether in 3 mg/kg dosage of CDDP or 1.5 mg/kg dosage of CDDP), which suggests a negative accumulation of CZACNs, CZAu, and CDDP@ZIF-90 in normal organs (Figure S14, Supporting Information).

Body weight and H&E staining of major organs imply that CZACNs have no systemic toxicity to the mice (Figure 6b and Figure S12, Supporting Information). However, we found that CDDP@ZIF-90, CZAu, and CZACN administration increased zinc dose in tumors when comparing them with CDDP and saline groups, which is attributed to the EPR effect (Figure 6c and Figure S13, Supporting Information). Moreover, zinc accumulation in tumors of CZACNs were the highest among other groups, resulted from the homologous target of cancer cell membrane coating. The results above confirmed CZACNs benefited from superior tumor accumulation in anticancer therapy. There were no significant changes in the serum levels of hepatic enzymes (ALT, AST, ALP, and LDH), or in kidney function markers (Urea and Crea) in the mice treated with CZACN compared to those of the saline group (Figure 6e and Figure S15, Supporting Information). In contrast, mice exposed to CDDP show renal damage. We emphatically found that CDDP treatment (whether high dosage or low dosage) both increased levels of Crea and Urea which are the typical indicators of renal function. We conclude that CZACNs decrease side effects of CDDP via efficient target to tumors, which is promising as a desirable therapeutic agent with good biocompatibility in vivo. It followed the safe use of our mitochondria-targeted nanoplatforms for combined chemo-photothermal therapy.

3. Conclusion

In summary, we developed an organelle specific anchored delivery system for combinational chemo-photothermal therapy by taking the most of the advantage of tumor hypoxia microenvironment. A ZIF-90-based nanoplatform equipped with cancer cell membrane coating and ATP-responsive encapsulation matrix, CDDP and Au nanozymes could be anchored to the mitochondria which is the main area of ATP production, and triggered a cascade reaction in mitochondria, eventually increasing the therapy efficiency and decreasing dose-limiting toxicity of CDDP. By virtue of the homologous target of cancer cell membrane and the photothermal conversion of Au nanozymes, the CZACNs surmounted two major problems widely existing in nanomedicine including distribution in normal tissues and solid tumor penetration. Therefore, the organelle-specific strategy highlights tailored translation potential for chemo-photothermal therapy.

Supporting Information

Supporting Information is available from the Wiley Online Library or from the author.

Acknowledgements

X.C., X.Y., and L.Z. contributed equally to this work. This work has been supported by the National Natural Science Foundation of China (22003038, 81922037, and 11575107), the Shanghai University-Universal Medical Imaging Diagnostic Research Foundation (19H00100), Shanghai Biomedical Science and Technology Support Project (19441903600), the Program for Changjiang Scholars and Innovative Research Team in University (IRT13078). The authors would like to thank the workers from Shiyanjia Lab (www.shiyanjia.com) for the ICP-OES analysis.

Conflict of Interest

The authors declare no conflict of interest.

Data Availability Statement

The data that support the findings of this study are available from the corresponding author upon reasonable request.

Keywords

biomimetic membrane coating, chemo-photothermal therapy, metal organic frameworks, organelle-specific, tumor hypoxia microenvironment

Received: August 27, 2021
Revised: November 25, 2021
Published online: December 19, 2021

[1] X. Guo, X. Wei, Z. Chen, X. Zhang, G. Yang, S. Zhou, *Prog. Mater. Sci.* **2020**, *107*, 100599.
[2] W. Jiang, C. A. von Roemeling, Y. Chen, Y. Qie, X. Liu, J. Chen, B. Y. S. Kim, *Nat. Biomed. Eng.* **2017**, *1*, 0029.

[3] M. A. Zanta, P. Belguise-Valladier, J. P. Behr, *Proc. Natl. Acad. Sci. U. S. A.* **1999**, *96*, 91.
[4] a) Y. Zhou, D. Zhang, G. He, C. Liu, Y. Tu, X. Li, Q. Zhang, X. Wu, R. Liu, *J. Mater. Chem. B* **2021**, *9*, 1009; b) J. He, C. Li, L. Ding, Y. Huang, X. Yin, J. Zhang, J. Zhang, C. Yao, M. Liang, R. P. Pirraco, J. Chen, Q. Lu, R. Baldridge, Y. Zhang, M. Wu, R. L. Reis, Y. Wang, *Adv. Mater.* **2019**, *31*, 1902409; c) Z. Lei, L. Ding, C. Yao, F. Mo, C. Li, Y. Huang, X. Yin, M. Li, J. Liu, Y. Zhang, C. Ling, Y. Wang, *Adv. Mater.* **2019**, *31*, 1807456.
[5] S. Rin Jean, D. V. Tulumello, S. P. Wisnovsky, E. K. Lei, M. P. Pereira, S. O. Kelley, *ACS Chem. Biol.* **2014**, *9*, 323.
[6] A. A. Khan, K. S. Allemailem, A. Almatroudi, S. A. Almatroodi, M. A. Alsahli, A. H. Rahmani, *J. Drug Delivery Sci. Technol.* **2021**, *61*, 102315.
[7] Q. Hu, M. Gao, G. Feng, B. Liu, *Angew. Chem., Int. Ed.* **2014**, *53*, 14225.
[8] X.-W. Ding, M. Robinson, R. Li, H. Aldhowayan, T. Geetha, J. R. Babu, *Pharmacol. Res.* **2021**, *171*, 105783.
[9] a) F.-K. Shieh, S.-C. Wang, C.-I. Yen, C.-C. Wu, S. Dutta, L.-Y. Chou, J. V. Morabito, P. Hu, M.-H. Hsu, K. C. W. Wu, C.-K. Tsung, *J. Am. Chem. Soc.* **2015**, *137*, 4276; b) X. Chen, R. Tong, Z. Shi, B. Yang, H. Liu, S. Ding, X. Wang, Q. Lei, J. Wu, W. Fang, *ACS Appl. Mater. Interfaces* **2018**, *10*, 2328.
[10] J. Chang, W. Lv, Q. Li, H. Li, F. Li, *Anal. Chem.* **2020**, *92*, 8959.
[11] H. Zhao, T. Li, C. Yao, Z. Gu, C. Liu, J. Li, D. Yang, *ACS Appl. Mater. Interfaces* **2021**, *13*, 6034.
[12] X. Chen, B. Liu, R. Tong, L. Zhan, X. Yin, X. Luo, Y. Huang, J. Zhang, W. He, Y. Wang, *Biomater. Sci.* **2021**, *9*, 590.
[13] Z. Shen, T. Liu, Y. Li, J. Lau, Z. Yang, W. Fan, Z. Zhou, C. Shi, C. Ke, V. I. Bregadze, S. K. Mandal, Y. Liu, Z. Li, T. Xue, G. Zhu, J. Munasinghe, G. Niu, A. Wu, X. Chen, *ACS Nano* **2018**, *12*, 11355.
[14] a) Y. Y. Yang, X. Liu, W. Ma, Q. Xu, G. Chen, Y. F. Wang, H. H. Xiao, N. Li, X. J. Liang, M. Yu, Z. Q. Yu, *Biomaterials* **2021**, *265*, 120456; b) D. Wang, C. Zhao, F. Xu, A. Zhang, M. Jin, K. Zhang, L. Liu, Q. Hua, J. Zhao, J. Liu, H. Yang, G. Huang, *Theranostics* **2021**, *11*, 2860.
[15] a) J. Ren, L. Zhang, J. Zhang, W. Zhang, Y. Cao, Z. Xu, H. Cui, Y. Kang, P. Xue, *Biomaterials* **2020**, *234*, 119771; b) H. Cheng, X.-Y. Jiang, R.-R. Zheng, S.-J. Zuo, L.-P. Zhao, G.-L. Fan, B.-R. Xie, X.-Y. Yu, S.-Y. Li, X.-Z. Zhang, *Biomaterials* **2019**, *195*, 75; c) M. Huo, L. Wang, Y. Chen, J. Shi, *Nat. Commun.* **2017**, *8*, 357.
[16] a) S. Wang, R. Chen, Q. Yu, W. Huang, P. Lai, J. Tang, L. Nie, *ACS Appl. Mater. Interfaces* **2020**, *12*, 45796; b) H.-B. Cheng, B. Qiao, H. Li, J. Cao, Y. Luo, K. M. K. Swamy, J. Zhao, Z. Wang, J. Y. Lee, X.-J. Liang, J. Yoon, *J. Am. Chem. Soc.* **2021**, *143*, 2413.
[17] a) R. Chen, S. Huang, T. Lin, H. Ma, W. Shan, F. Duan, J. Lv, J. Zhang, L. Ren, L. Nie, *Nat. Nanotechnol.* **2021**, *16*, 455; b) J. Lv, S. Li, J. Zhang, F. Duan, Z. Wu, R. Chen, M. Chen, S. Huang, H. Ma, L. Nie, *Theranostics* **2020**, *10*, 816; c) Z. Zheng, H. Liu, S. Zhai, H. Zhang, G. Shan, R. T. K. Kwok, C. Ma, H. H. Y. Sung, I. D. Williams, J. W. Y. Lam, K. S. Wong, X. Hu, B. Z. Tang, *Chem. Sci.* **2020**, *11*, 2494.
[18] a) N. Zhang, M. Li, X. Sun, H. Jia, W. Liu, *Biomaterials* **2018**, *159*, 25; b) L. Rao, Q.-F. Meng, Q. Huang, P. Liu, L.-L. Bu, K. K. Kondamareddy, S.-S. Guo, W. Liu, X.-Z. Zhao, *Adv. Healthcare Mater.* **2016**, *5*, 648; c) K. Cheung-Ong, G. Giaever, C. Nislow, *Chem. Biol.* **2013**, *20*, 648.
[19] S. Dasari, P. B. Tchounwou, *Eur. J. Pharmacol.* **2014**, *740*, 364.
[20] H. S. Oberoi, N. V. Nukolova, A. V. Kabanov, T. K. Bronich, *Adv. Drug Delivery Rev.* **2013**, *65*, 1667.